2021-2

Lithium Niobate Fabry-Perot microcavity based on strip loaded waveguides

Maria V. Kotlyar
Centre for Advanced Photonics and Process Analysis, Munster Technological University, Cork, Ireland; Tyndall National Institute, Cork, Ireland, maria.kotlyar@mtu.ie

Simone Iadanza
Centre for Advanced Photonics and Process Analysis, Munster Technological University, Cork, Ireland; Tyndall National Institute, Cork, Ireland, Simone.Iadanza@mtu.ie

Liam O'Faolain
Centre for Advanced Photonics and Process Analysis, Munster Technological Universit, Cork, Ireland; Tyndall National Institute, Cork, Ireland, liam.ofaolain@tyndall.ie

Recommended Citation

Kotlyar, M.V., Iadanza, S. and O'Faolain, L. (2021). Lithium Niobate Fabry-Perot microcavity based on strip loaded waveguides. Photonics and Nanostructures - Fundamentals and Applications, [online] 43, p.100886. doi:https://doi.org/10.1016/j.photonics.2020.100886.

Photonics and Nanostructures - Fundamentals and Applications 43 (2021) 100886

Contents lists available at ScienceDirect

Photonics and Nanostructures - Fundamentals and Applications

journal homepage: www.elsevier.com/locate/photonics

Lithium Niobate Fabry-Perot microcavity based on strip loaded waveguides

Maria V. Kotlyar [a,b,*], Simone Iadanza [a,b], Liam O'Faolain [a,b]

[a] Centre for Advanced Photonics and Process Analysis, Cork Institute of Technology, Cork, Ireland
[b] Tyndall National Institute, Cork, Ireland

ARTICLE INFO

Keywords:
Lithium niobate
Silicon nitride
Fabry-Perot
Bragg grating

ABSTRACT

In this work, we combine Lithium Niobate on insulator with a silicon nitride layer to form strip-loaded waveguides that can take advantage of the strong nonlinear optical coefficients of lithium niobate and of the high refractive contrast and ease of processing of silicon nitride. We describe the design and fabrication of a Fabry-Perot cavity formed by Distributed Bragg Reflectors. We discuss the design trade-offs implicit in the realisation of such microcavities of this nature and demonstrate an experimental quality factor of 2300, which is to our knowledge, the highest experimentally reported result for such type of waveguide based Fabry-Perot cavity.

1. Introduction

Photonic integrated circuits (PICs) have emerged as a mature and industrially relevant platform in the last decades. Photonic devices offer several advantages compared to electronics, such as a large bandwidth of operation, wavelength division multiplexing, and absence of electromagnetic interference. PICs are also enabling the integration of passive and active optical components on a single chip.

Silicon on insulator (SOI) [1], silicon nitride (SiN) [2], indium phosphate (InP) [3] and lithium niobate (LN) [4] are materials used extensively for PIC platforms. Among these materials, LN is one of the most popular materials for nonlinear optics due to its strong second-order nonlinear effect. It also has excellent electro-optic and acousto-optic properties and a low-loss transparency window, spanning from visible to mid infrared. LN can be doped with rare-earth ions to realise amplification [5].

LN based modulators and switches have been vital to the development of optical telecommunications [6,7]. Periodically-poled LN (PPLN) has been central to the development of numerous nonlinear devices, such as optical frequency converters and parametric oscillators [8,9]. LN has been used in many other applications as well, such as Q-switches for lasers [10], and as entangled photon-pair sources for quantum optics applications [11].

However, LN is extremely difficult to process which typically limits applications to the use of bulk crystals of large mode area, low refractive index contrast waveguides. Consequently, typical devices remain bulky (often centimetres long), expensive and require high-power electrical drivers [12].

Recent advances in fabrication technologies allowed the realisation of lithium niobate on Insulator (LNOI) material [13], which facilitates the creation of compact integrated devices such as photonic nanowires [14], microdisk and microring resonators [15,16], photonic crystals [17] and integrated grating couplers [18].

LN propagation losses of the same order of magnitude (few dB/m) as that of its semiconductor counterparts were achieved recently in photonic wires [19]. The largest quality factor for on - chip LN microresonators reported so far is 1.6×10^{7} which was demonstrated by Wu et al. [20] in LN microdisks. However, microdisks exhibit a low free spectal range, which limits their range of applications. The use of two-dimentional LN-based photonic crystals with a tight mode confinement and high quality-factor allowed observation of third harmonic generation in on-chip LN device [21].

In this paper, a LNOI on Si wafer was combined with silicon nitride layer to form strip-loaded waveguides that take advantage of the strong nonlinear optical coefficients of lithium niobate and of the high refractive contrast and ease of processing of silicon nitride. This approach has the advantage of being substrate based (as opposed to membraned or free standing structures) increasing the potential for integration with other devices and systems. We developed, fabricated and characterised a Fabry-Perot micro-cavity in such material for the first time. The Fabry-perot micro-cavity offers a high ease of fabrication, even mode spacing and excellent control over the free spectral range, which is advantageous for applications such as parametric down conversion amongst others.

* Corresponding author at: Centre for Advanced Photonics and Process Analysis, Cork Institute of Technology, Cork, Ireland.
E-mail addresses: Maria.kotlyar@cit.ie (M.V. Kotlyar), Simone.iadanza@mycit.ie (S. Iadanza), Liam.ofaolain@tyndall.ie (L. O'Faolain).

https://doi.org/10.1016/j.photonics.2020.100886
Received 17 September 2020; Received in revised form 23 November 2020; Accepted 25 November 2020
Available online 1 December 2020

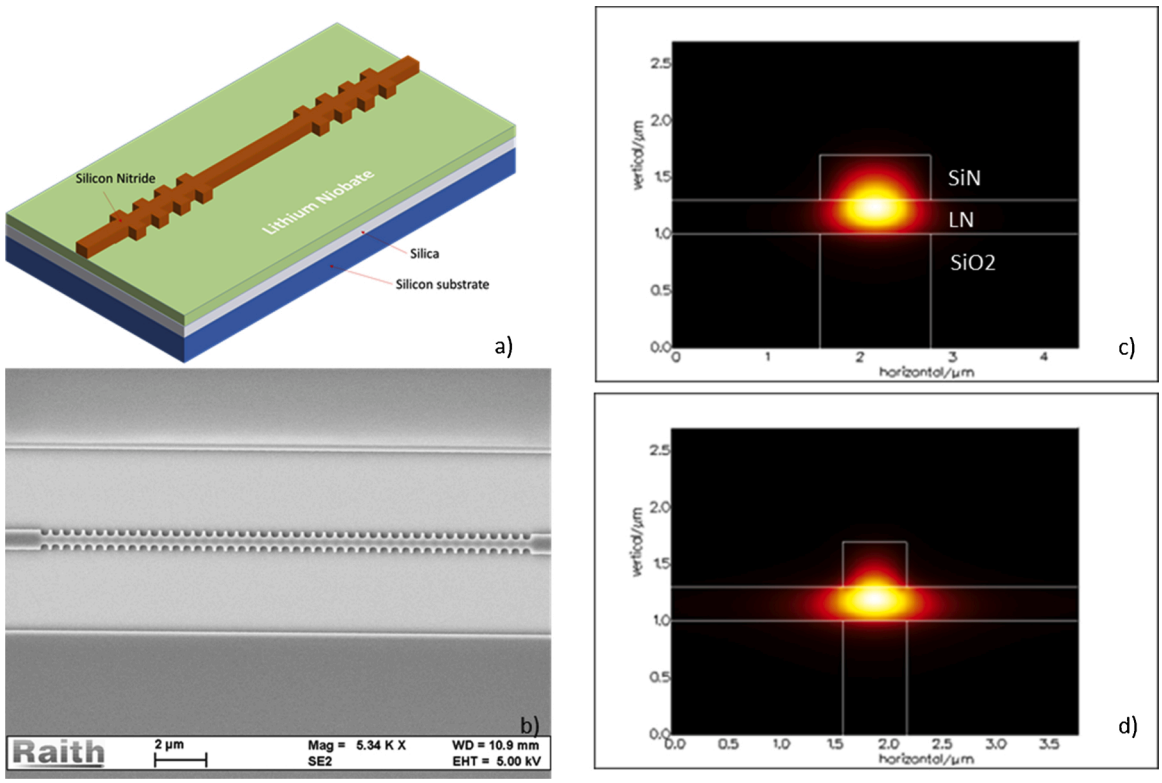

Fig. 1. a) Schematic of a device consisting of a FP cavity formed by DBRs, which consist of sections with alternating widths of silicon nitride. b) The SEM image of the top view of DBRs. c,d) Simulations showing the mode shape for both sections of DBRs.

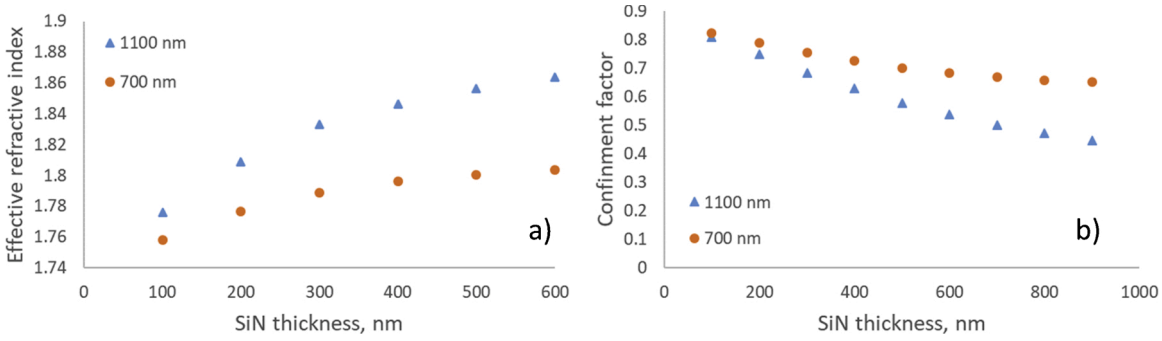

Fig. 2. a) Effective refractive index of the mode for two sections of DBR mirrors as a function of SiN thickness, b) Mode confinement factor in LN layer vs SiN thickness.

2. Device structure and simulations

A Fabry-Perot (F-P) cavity with Distributed Bragg Reflectors (DBR) providing mirrors on both sides of the cavity in LNOI material was studied in our work. At its simplest, a Bragg grating is a structure with a periodic modulation of the effective refractive index in the propagation direction of the optical mode. This modulation can be achieved by alternating either materials or the physical dimensions of the waveguide. Here we employed sidewall-width modulated structures with rectangular corrugations (Fig. 1a, b).

A cross-section of our strip-loaded waveguide is presented in Fig. 1c, d. The thickness of LN was chosen to be as small as possible to maximise the change in refractive index in Bragg mirror sections. We used a value of 300 nm as this was the limit of the current fabrication process; thinner layers exhibit poorer uniformity. The DBR is realised by the deposition and patterning of a silicon nitride layer. In this way, the LN left unpatterned, thus minimising losses; a point which will be discussed further in fabrication section.

A thickness of SiN of 400-nm provides a good compromise between a relatively large effective refractive index difference for the grating sections ($\Delta n \sim 0.05$) while still keeping a large fraction of the mode confined within LN layer (60–75 %) (Fig. 2a,b). A thickness of 400-nm for SiN film is also close to its fabrication limit of our process, as thicker layer are highly stressed and could de-laminate. In Fig. 2a, we plot the effective refractive index with varying SiN layer thickness for two different SiN widths of 1100 nm and 700 nm, which are the chosen widths of waveguides creating Bragg gratings. We found that for widths greater than 1200 nm, the waveguide supported a second mode. For corrugations above 400 nm, losses for F-P were increased, and hence we chose widths of 1100 and 700 nm for the grating sections. Fig. 1(c, d) shows simulated TE modes for both widths of the grating (1100 and 700 nm). As one can see, for the narrow waveguides of 700 nm, a larger part of the mode is confined to LN layer compared to 1100-nm wide waveguide allowing us to change effective refractive index of the structure. All the simulations above were carried out using the commercial software PhotonDesign FIMMPROP.

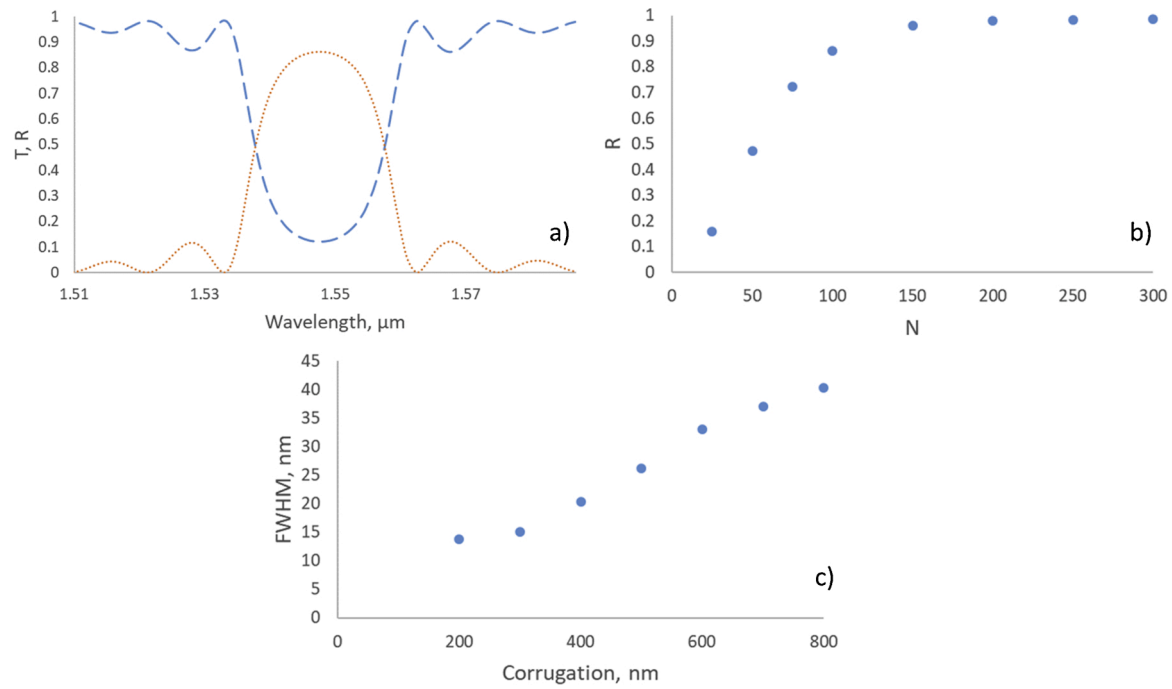

Fig. 3. a) Transmission (dashed) and reflection (dotted) spectrum for DBRs consisting of 150 periods with 400 nm corrugation, b) Maximum reflection as a function of number of periods, c) Full width at half maximum of the stop-band as a function of the corrugation of the DBR.

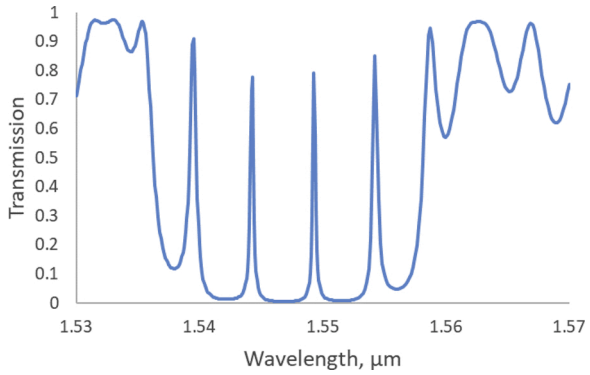

Fig. 4. Simulated transmission spectrum of a 85.2 μm long FP cavity with DBRs consisting of 100 periods on each side of the cavity.

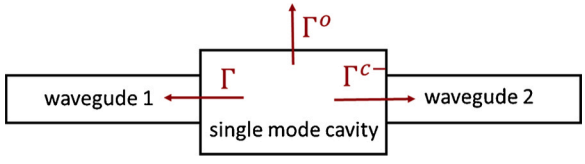

Fig. 5. A schematic representation of two waveguides coupled together via a high Q resonator.

Simulated transmission and reflection spectra for the DBR with the parameters chosen above are presented in Fig. 3(a). We chose a period of the grating of 426 nm so that the middle of the band-gap is centred around the telecommunication wavelength of 1550 nm. Fig. 3b shows that it was possible to achieve almost 100 % of reflection with about 200 periods. Regarding the stop band width, we selected FWHM of around 20 nm (Fig. 3c) which corresponds to delta n of 0.05 and amplitude of corrugation of 400 nm. We found these numbers to provide the best trade-off between depth of corrugation, single mode operation and low scattering, which increases with decreasing width of the narrow section of the grating.

The length of F-P cavity was chosen to be 85.2 μm. This cavity length corresponds to free spectral range of approximately 5 nm and provides at least 2 transmission peaks within the stopband.

Fig. 4 shows a simulated spectrum of such F-P with 100 Bragg gratings on each side.

Let us consider our device as waveguide-resonator coupling system as shown schematically in Fig. 5. In this case, we can use scattering theory [22] to find analytically scattering amplitudes of the cavity. In Fig. 5 Γ^0 represents the intrinsic cavity loss and Γ^c represents the cavity decay rate into waveguides and it is the same for both waveguides, when the number of periods in each DBR is kept constant ($\Gamma^{c+} = \Gamma^{c-} = \Gamma^c/2$).

In terms of quality factors of the cavity Q, which are inversely proportional to Γ, and considering operation at the resonant wavelengths, one can use following formulas to express the transmittance (T) and reflectance (R) as functions of Q factors of the cavity (the detailed derivation of these formulas is given by Yariv et al. in [22]):

$$T = \frac{Q_{total}^2}{Q_c^2}\ ,\ R = \frac{Q_{total}^2}{Q_o^2} \tag{1}$$

Where Q_c depends on the coupling efficiency between the waveguides and cavity mode, Q_o is associated with light scattered out of the cavity and is called intrinsic quality factor of the cavity, Q_{total} is a total quality factor of the cavity and depends on two other quality factors in following way $\frac{1}{Q_{total}} = \frac{1}{Q_c} + \frac{1}{Q_o}$.

Q_c is controlled via a number of periods in Bragg gratings. Q_o is a function of the design and ultimately of the fabrication process. It is important to realise that a trade-off exists between Q_{total} and transmission as we can see from Fig. 6(a, b).

As can be seen from Fig. 6(a) both Q_c and Q_o are functions of the number of mirror sections, N. Increasing N creates a slow increase in total quality factor Q_{total} until it saturates after N = 250. Q_c grows exponentially with increasing N, causing a rapid decrease in transmission, illustrating that it is impossible to achieve high Q_{total} and high T simultaneously (Fig. 6b). Different figures of merit (as a function of the T and Q_{total}) can be calculated for different applications, though most will

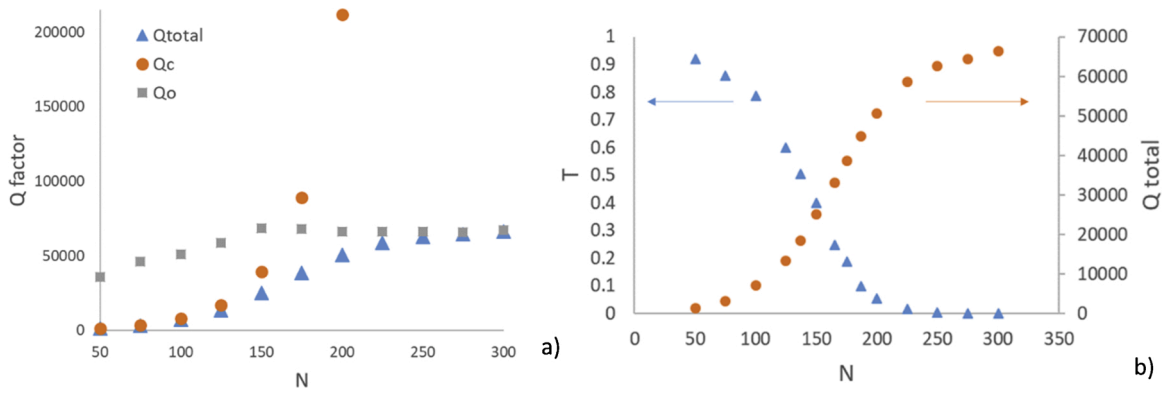

Fig. 6. a) Simulated Q factors of the cavity as functions of number of periods in the DBR, b) Total Q factor and transmission at a Bragg wavelength as functions of number of periods.

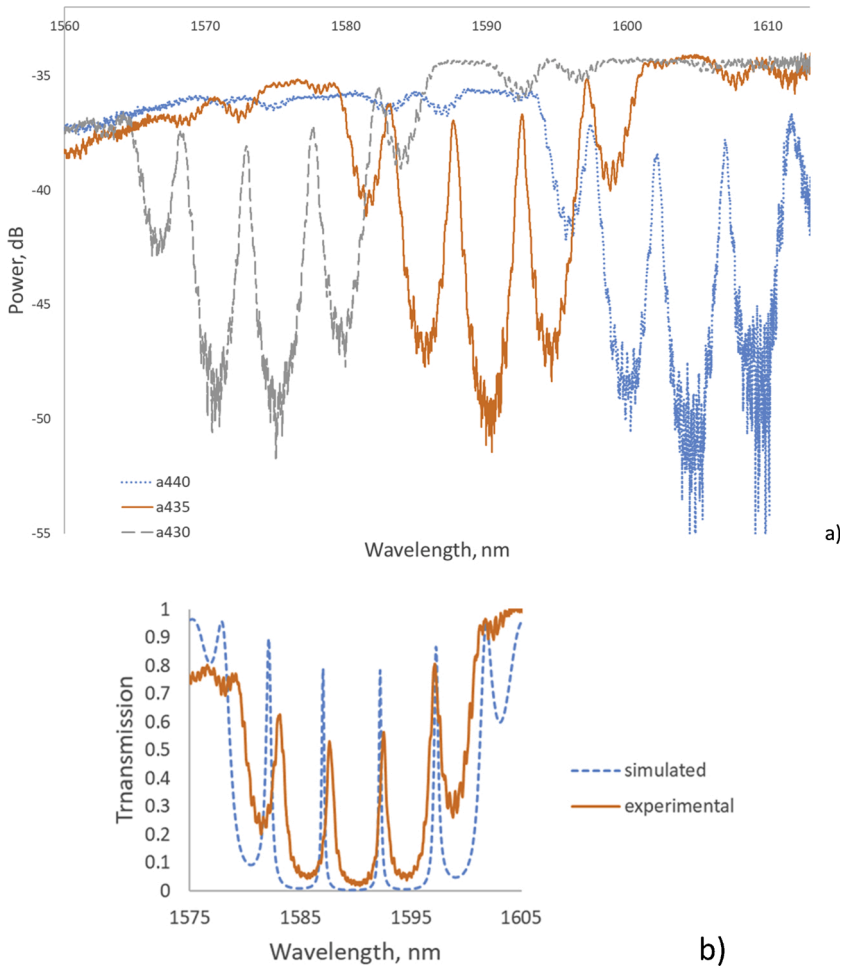

Fig. 7. a) Experimental transmission spectrum of FP cavities formed by DBRs with different periods, plotted on a logarithmic scale. b) Comparison of a simulated and experimental transmission spectrum (normalized to the transmission of a waveguide without the cavity) of the same period of 435 nm.

show a maximum point for 150–175 mirrors.

3. Fabrication and experiment

We selected a commercially available X-cut LNOI wafer fabricated by NANOLN (Jinan Jingzheng Electronics Co., Ltd.) as the material for our experiments. The wafer was produced by the ion-slicing technique [23] with 300 nm of LN bonded to a 2 μm thick SiO2 layer grown on a Si substrate (Fig. 1c, d). The deposition of the 400 nm-thick SiN film was carried out in a commercial available Plasma Enhanced Chemical Vapour Deposition (PECVD) system model STS (Surface Technology Systems), which is a capacitively coupled parallel plate reactor driven by a 13.56 MHz high frequency (HF) and 187 kHz low frequency (LF) power supply. The temperature of the substrate holder was 300 °C. The precursor gases for the deposition of SiN film were silane (SiH4), and ammonia (NH3) with nitrogen (N2) as diluent gas. The pressure in the chamber was kept at 900 m T. 450 nm of ZEON ZEP-520A was spun on the top of SiN to serve as both an etch mask for the patterning of SiN and

Table 1
Comparison of quality factors of experimental and simulated cavities of length 87 μm and grating period of 435 nm.

Method	Qtotal	Qo	Qc
Experiment	2281	10,564	2910
Simulation	6922	58,972	7843

as an electron-beam resist. Electron beam lithography (EBL) was performed by a RAITH eLINE system. The resist pattern was then transferred into a SiN layer via ICP (Oxford STS) in a mixture of CHF3 and SF6 gases at room temperature. The remaining hardened ZEP mask was stripped off the sample in 1165 solvent at 90 °C. Light with Transverse Electric (TE) polarisation from a broad-band source operating between 1500 and 1620 nm was launched into the input waveguide using a lens, another lens collected the light at the output of the device and sent it into a detector. The single bend of radius 100 μm of the input waveguides was also introduced for preventing the direct light from the source from entering the objective lens located in front of the detector. An optical spectrum analyser was used to record the transmission spectra of devices for three different DBR periods with N = 100 mirrors. These are presented in Fig. 7(a) on a logarithmic scale.

As one can see from the Fig. 7a extinction ration of the filter was around 15 dB. The extinction ratio can be improved further by optimising the grating design and fabrication process, thus minimising the losses and improving the Q_0 value. Fig. 7b shows a comparison of the experimental spectrum for a Fabry-Perot microcavity with length of 87 μm and grating period 435 nm with simulated results. Using formula (1) we calculated various quality factors from the experimental spectrum in Fig. 7b and compared them to simulated values at a wavelength of around 1592 nm (see Table 1)

The reduced quality factors of the experiment relative to simulations is due to imperfections of the fabrication process. The square profile of the simulated Bragg grating was smoother and rounder in the fabricated device (see Fig. 1b). Fabrication also caused extra roughness which resulted in extra scattering losses.

4. Conclusions

We have described the design and fabrication of a F-P cavity with Bragg gratings in silicon nitride LNOI strip-loaded waveguides. We have discussed the design trade-offs implicit in the realisation of microcavities of this nature. To our knowledge the experimental quality factor of 2300 is highest experimentally reported result for such type of F-P cavity in LNOI in a strip-loaded type waveguide. Further improvements in Q-factors can be achieved by implementing gentle confinement similar to that employed in [24]. These compact lithium niobate F-P microcavities will be a powerful tool for the realization of important functions such as on chip parametric down conversion and second harmonic generation.

Declaration of Competing Interest

The authors report no declarations of interest.

Acknowledgments

This work was supported by a European Commission Horizon 2020 Marie Skłodowska-Curie Fellowship "TERRIFIC" grant agreement no. 749143 and by the Science Foundation Ireland under Grant SFI 12/RC/2276 and Grant SFI 16/ERCS/3838;

References

[1] J. Leuthold, C. Koos, W. Freude, Nonlinear silicon photonics, Nat. Photonics 4 (2010) 535–544.
[2] D.J. Moss, R. Morandotti, A.L. Gaeta, M. Lipson, New CMOS-compatible platforms based on silicon nitride and Hydex for nonlinear optics, Nat. Photonics 7 (2013) 597–607.
[3] F.A. Kish, David Welch, Radhakrishnan Nagarajan, Jacco L. Pleumeekers, Vikrant Lal, Mehrdad Ziari, Alan Nilsson, Masaki, et al., Current status of large-scale InP photonic integrated circuits, IEEE JSTQE 17 (2011) 1470–1489.
[4] E.L. Wooten, K.M. Kissa, A. Yi-Yan, E.J. Murphy, D.A. Lafaw, P.F. Hallemeier, D. Maack, D.V. Attanasio, D.J. Fritz, G.J. McBrien, D.E. Bossi, A review of lithium niobate modulators for fiber-optic communications systems, IEEE J. Sel. Top. Quantum Electron. 6 (1) (2000) 69–82.
[5] W. Sohler, B. Das, D. Dey, S. Reza, H. Suche, R. Ricken, Erbium-doped lithium niobate waveguides lasers, IEICE Trans. Electron. E88 (C) (2005) 990–997.
[6] M. Izutsu, Y. Yamane, T. Sueta, Broad-band traveling-wave modulator using a LiNbO3 optical waveguide, IEEE J. Quantum Electron. 13 (4) (1977) 287–290.
[7] H. Nishimoto, M. Iwasaki, S. Suzuki, M. Konodo, Polarization independent LiNbO3 8 × 8 matrix switch, IEEE Photonics Technol. Lett. 2 (9) (1990) 634–636.
[8] L.E. Myers, G.D. Miller, R.C. Eckardt, M.M. Fejer, R.L. Byer, W.R. Bosenberg, Quasi-phase-matched 1.064-μm-pumped optical parametric oscillator in bulk periodically poled LiNbO3, Opt. Lett. 20 (1) (1995) 52–54.
[9] E.J. Lim, M.M. Fejer, R.L. Byer, Second-harmonic generation of green light in periodically poled planar lithium niobate waveguide, Electron. Lett. 25 (3) (1989) 174–175.
[10] S.T. Lin, G.W. Chang, Y.Y. Lin, Y.C. Huang, A.C. Chiang, Y.H. Chen, Monolithically integrated laser Bragg Q-switch and wavelength converter in a PPLN crystal, Opt. Exp. 15 (25) (2007) 17093–17098.
[11] S. Tanzilli, H. de Riedmatten, W. Tittel, H. Zbinden, P. Baldi, M. de Micheli, D. B. Ostrowski, N. Gisin, Highly efficient photon-pair source using periodically poled lithium niobate waveguide, Electron. Lett. 37 (1) (2001) 26–28.
[12] D. Janner, D. Tulli, M. García-Granda, M. Belmonte, V. Pruneri, Micro-structured integrated electro-optic LiNbO3 modulators, Laser Photonics Rev. 3 (3) (2009) 301–313.
[13] P. Rabiei, P. Gunter, Optical and electro-optical properties of submicrometer lithium niobate slab waveguides prepared by crystal ion slicing and wafer bonding, Appl. Phys. Lett. 85 (20) (2004) 4603–4605.
[14] H. Hu, R. Ricken, W. Sohler, Lithium niobate photonic wires, Opt. Express 17 (26) (2009) 24261–24268.
[15] J. Wang, F. Bo, S. Wan, W. Li, F. Gao, J. Li, G. Zhang, J. Xu, High-Q lithium niobate microdisk resonators on a chip for efficient electro-optic modulation, Opt. Express 23 (18) (2015) 23072–23078.
[16] S.Y. Siew, S.S. Saha, M. Tsang, A.J. Danner, Rib microring resonators in Lithium niobate on insulator, IEEE Photonics Technol. Lett. 28 (5) (2016) 573–576.
[17] L. Cai, S. Zhang, H. Hu, A compact photonic crystal micro-cavity on a single-mode lithium niobate photonic wire, J. Opt. 18 (3) (2016), 035801.
[18] M.S. Nisar, X. Zhao, A. Pan, S. Yuan, J. Xia, Grating coupler for an on-chip Lithium niobate ridge waveguide, IEEE Photonics J. 9 (1) (2017) 1–8.
[19] R. Wu, Long low-loss-Litium niobate on insulator waveguides with sub-nanometer surface roughness, Nanomaterials Basel (Basel) 8 (11) (2018) 910.
[20] R. Wu, J. Zhang, N. Yao, W. Fang, L. Qiao, Z. Chai, J. Lin, Y. Cheng, Lithium niobate micro-disk resonators of quality factors above 10^7, Opt. Lett. 43 (2018) 4116.
[21] Mingxiao Li, High-Q two-dimensional lithium niobate photonic crystal slab nanoresonators, Nanomaterials 8 (2018) 910.
[22] Yong Xu, Yi Li, Reginald K. Lee, Amnon Yariv, Scattering-theory analysis of waveguide-resonator coupling, Phys. Rev. E Stat. Phys. Plasmas Fluids Relat. Interdiscip. Topics 62 (5) (2000) 7389.
[23] G. Poberaj, H. Hu, W. Sohler, P. Günter, Lithium niobate on insulator (LNOI) for micro-photonic devices, Laser Photonics Rev. 1- (16) (2012).
[24] Su-Peng Yu, Hojoong Jung, Travis C. Briles, Kartik Srinivasan, Scott B. Papp, Photonic-crystal-reflector nanoresonators for kerr-frequency combs, ACS Photonics 6 (8) (2019) 2083–2089.